Sensors and Materials, Vol. 11, No. 8 (1999) 479–492
MYU Tokyo

S & M 0390

Piezoresistive Accelerometer Fabricated by Selective Formation and Etching of Porous Silicon

Jun-Hwan Sim, Chan-Seob Cho [1], Jin-Sup Kim [2],
Jung-Hee Lee [3] and Jong-Hyun Lee [3]

Department of Electronics & Communication Engineering, Korea Maritime University,
Pusan 606-791, Korea
[1] Department of Electronic & Electrical Engineering, Sangju National Polytech. University,
Sangju 742-170, Korea
[2] Department of Electronic Engineering, Inje University, Kimhae 621-749, Korea
[3] School of Electronic & Electrical Engineering, Kyungpook National University,
Taegu 702-701, Korea

(Received March 16, 1998; accepted October 5, 1999)

Key words: silicon micromachining, porous silicon etching, eight-beam structure, piezoresistive silicon accelerometer

This is a report on the selective formation and etching of porous silicon, and the fabrication of a piezoresistive silicon accelerometer with eight beams on a selectively diffused (111)-oriented n/n$^+$/n substrate using a porous silicon micromachining technique. This technique has many of the advantages of both bulk and surface micromachining without their disadvantages, and is capable of precisely constructing a microstructure by defining the n$^+$-diffusion region and patterning the n-epitaxial layer, thereby, avoiding any lateral etching or undercutting. Through the use of an eight-beam structure, the mechanical strength of the accelerometer could be greatly improved due to a smaller shear stress. The lower sensitivity of the sensor was easily adjusted by combining the four output signals of the four half-bridges. The effectiveness of the sensor was confirmed through an experiment in which the accelerometer was characterized.

1. Introduction

Silicon accelerometers have some attractive features such as small size, low cost and mass-production capabilities with standard IC technologies.[1,2] Recently, the development of many kinds of silicon accelerometers based on piezoresistive, capacitive, and other

sensing principles, have been reported.[3–6] These sensors are mainly fabricated using either bulk or surface micromachining techniques.[7,8]

Bulk micromachining is normally conducted using isotropic chemical etching solutions. To achieve a high-resolution etch and precise dimensional controllability, some additional special techniques such as deep etching, two-sided (front-back) etching, or anodic bonding are often adopted, which result in a low yield and high cost of the device fabrication. Surface micromachining usually utilizes deposited polycrystalline silicon as a structural or sacrificial layer, which is subsequently patterned and etched away to construct the desired structure. However, polycrystalline silicon, which is widely used in surface micromachining, has poor mechanical properties compared to those of single-crystalline silicon and consequently, the film quality is closely related to the specific deposition conditions.

Alternative surface micromachining techniques using a porous silicon etching technique have been suggested, since these would not suffer from the problems mentioned above. Porous silicon is formed by the electrochemical dissolution of monocrystalline silicon in hydrofluoric (HF) acid. Since the porous silicon formation is strongly dependent on both the substrate type and the doping level,[9] several methods for the selective formation of a porous silicon layer and the subsequent etching of the layer have been investigated.[10–12] However, the method described by Tu[10] requires several repetitious implantations with proton and nitrogen, and it is also difficult to define the side of the microstructure. Other methods using the n/p substrate, developed by Eijkel *et al.*[11] and Lang *et al.*,[12] were shown to have difficulties in controlling the air gap between the microstructure and the substrate and with the definition of the exact geometry of the microstructure, due to undesirable undercutting caused by the isotropic anodic reaction.

A bridge-type accelerometer, which can support the mass in eight directions, has not been introduced up to now because of the difficulty in the precise shaping of the microstructure using a conventional isotropic silicon etching process and due to the lower sensitivity of the structure than that of a two- or four-beam bridge-type accelerometer. However, an eight-beam structure offers a lower cross-axis sensitivity to lateral acceleration parallel to the device surface than a two- or four-beam structure.

In this study, we present a highly selective, self-stopping[13] porous silicon surface micromachining technique which is more effective for controlling the air gap height, the beam thickness, and the shape of the microstructure due to the selective formation of n^+-porous silicon in a selectively diffused (111)-oriented $n/n^+/n$ substrate. We will also describe the detailed fabrication process and the experimental results of the production of a piezoresistive silicon accelerometer with eight beams, using porous silicon micromachining.

2. Porous Silicon Micromachining

In this section, two different processes are presented for the fabrication of free-standing microstructures. The first fabrication process is shown in Fig. 1. It begins with the diffusion of a highly doped n^+ layer over an n-type substrate and the subsequent growth of a lightly doped n-epitaxial layer. Next, three-dimensional structures are patterned by dry

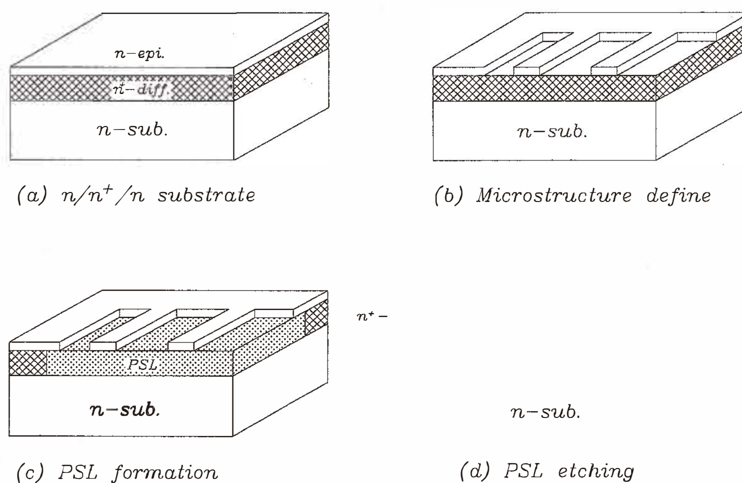

Fig. 1. Process sequence for fabricating silicon microstructures using a porous silicon etching method.

etching or wet chemical etching through the epitaxial layer. These structures are then freed from the substrate by forming, and subsequently dissolving porous silicon in portions of the n$^+$ layer.

Figure 2 shows a scanning electron microscopy (SEM) micrograph of a free-standing cross with a 5 μm thickness, 5 μm width, and 200 μm length, fabricated by porous silicon etching on a blank diffused (111)-oriented n/n$^+$/n substrate. A porous silicon layer was formed on a 20-μm-thick n$^+$-nonselectively diffused layer by anodization in a 20% aqueous HF solution. Then a current density of 10 mA/cm^2 was applied for 5 min at room temperature. After the porous silicon layer was removed in a 5 wt% NaOH solution, a completely undercut cross pattern with a uniform thickness and no cusp was observed. Since the dopant concentration in the n$^+$-diffused layer was much higher than that in the n-epitaxial layer and the substrate, the anodic reaction occurred only in the n$^+$-diffused layer. However, during the reaction, porous silicon etching spread laterally into the n$^+$ region beneath the edge of the n-epitaxial layer, which caused undesirable undercutting as the n$^+$ layer became diffused over the entire n-type substrate.

For application in sensors, a microstructure must have exactly defined areas without any lateral undercut. This can be successfully achieved using a selectively diffused (111)-oriented n/n$^+$/n substrate, as shown in Fig. 3. Figure 4 shows SEM micrographs of cantilevers fabricated by the selective formation and etching of porous silicon in a selectively diffused n/n$^+$/n silicon substrate. The widths are 30, 50, 70, and 100 μm, and the lengths and thicknesses are all 700 μm. Step 1 in Fig. 4 is the result of isotropic silicon etching through an n-epitaxial layer, which reveals the n$^+$-diffused layer, and step 2 is the

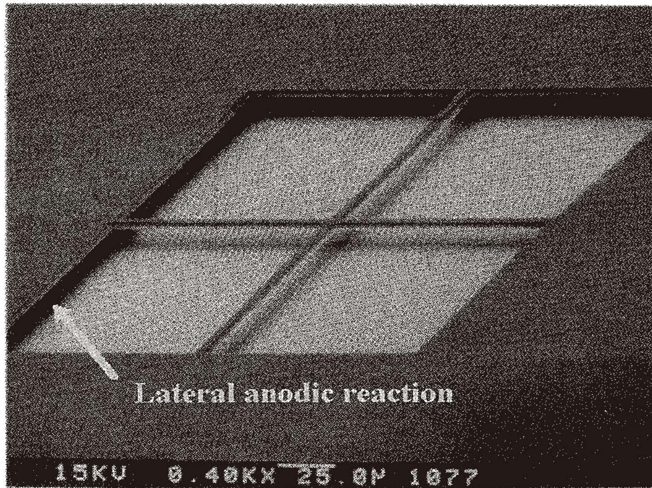

Fig. 2. SEM micrograph of a 5-μm-thick, 5-μm-wide, and 200-μm-long free-standing cross fabricated by porous silicon etching.

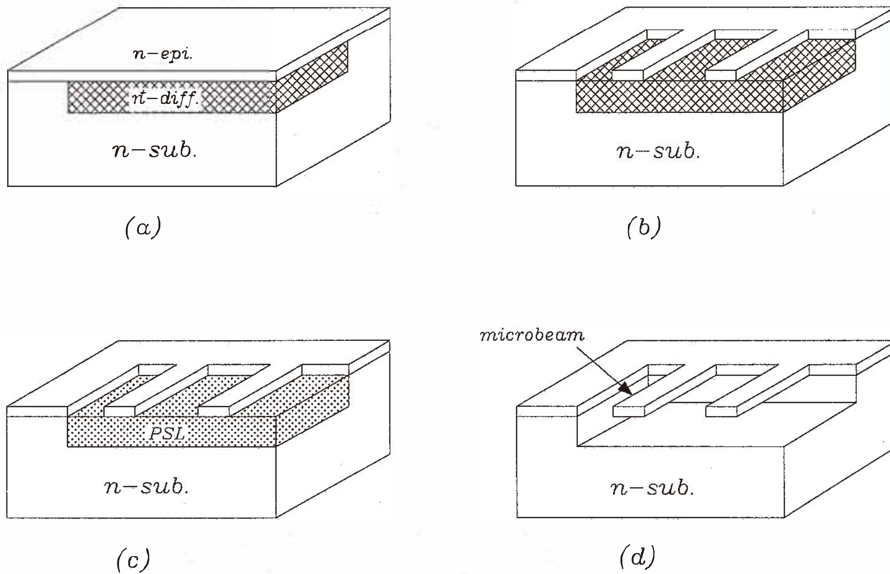

Fig. 3. Process flow for free-standing microstructures fabricated using a selectively diffused n/n$^+$/n silicon substrate. (a) Formation of a selectively diffused n/n$^+$/n multilayer, (b) definition of three-dimensional structures by reactive ion etching (RIE) or wet chemical etching, (c) selective conversion of an n$^+$ layer to a porous silicon layer, and (d) removal of a porous silicon layer in a weak NaOH solution to form free-standing structures.

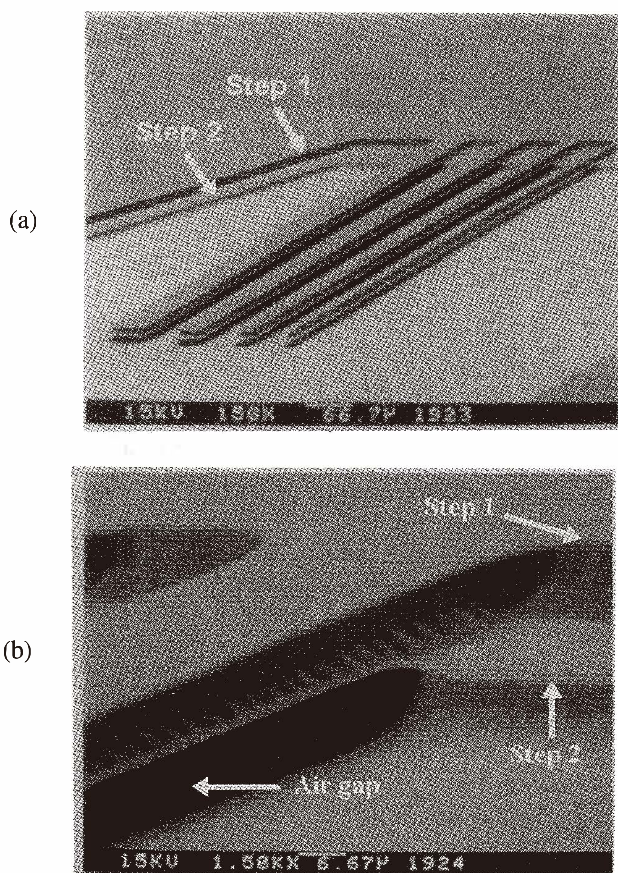

Fig. 4. SEM micrographs of cantilevers fabricated by selective formation and the etching of porous silicon. (a) Free-standing cantilevers with various widths and (b) close-up of a connecting part between a cantilever and the substrate.

edge between the n^+-diffusion region and the n-substrate. Since the n^+-region was selectively diffused on the n-silicon substrate, the porous silicon was formed only in the n^+-region through an anodic reaction, as shown in Fig. 4(b), while the lightly doped epitaxial silicon and substrate provided etch stops. The undesirable undercutting phenomenon of the microstructure shown in Fig. 2 was, therefore, not observed in the $n/n^+/n$ structure with a buried n^+ layer. Consequently, we were able to precisely control the dimensions of the microstructures by defining the n^+-diffusion region and patterning the n-epitaxial layer. For this reason, porous silicon micromachining was used in the fabrication of the microstructure of an accelerometer, as discussed below.

3. Fabrication of Piezoresistive Accelerometer

3.1 *Experimental*

The detailed procedure for the fabrication of a silicon accelerometer is shown in Fig. 5. (111)-Oriented, 5–10 Ωcm, n-type silicon wafers were used as starting materials. A 0.8-μm-thick silicon dioxide masking layer was thermally grown and patterned. Then a 20-μm-thick n^+-region, which served as a sacrificial layer and provided an air gap, was selectively formed by deep phosphorous diffusion. The resultant doping density of the n^+-buried layer, confirmed by a spreading resistance measurement, was above 1×10^{17}/cm^3, which was high enough to be anodizable in a HF solution. A low-doped n-type epitaxial layer with an As doping density of 5×10^{15}/cm^3, which is used as a movable microstructure, was then deposited on the substrate (Fig. 5(a)).

Another thin surface oxide was thermally grown on a low-doped n-epitaxial layer. The piezoresistors were formed by boron ion implantation with a dose of 2.7×10^{14} cm^{-2} at 40 keV through a thin surface oxide which was followed by annealing at 1,070°C for 70 min in N_2 atmosphere (Fig. 5(b)). The measured junction depth and sheet resistance of the piezoresistors were about 1 μm and 240 Ω/□, respectively. After 1,000-Å-thick passivation oxide and 1,500-Å-thick stress-relief nitride were both deposited, the back of the wafer was heavily implanted with phosphorus to ensure a uniform current density during anodization (Fig. 5(c)).

A 1,000-Å-thick Ni-Cr glue layer and 6,000-Å-thick Au layer were sequentially deposited by e-beam evaporation and then patterned by wet etching as the masking layer for anodization. In order to provide a pass for anodization, the uncovered parts of the nitride and oxide layers were removed by plasma and wet chemical etching, respectively, and the n-epitaxial silicon layer was etched to a depth of 8 μm using reactive ion etching (RIE). A 1-μm-thick aluminum back ohmic contact was deposited by e-beam evaporation (Fig. 5(d)).

The anodic reaction was performed in a 10% aqueous HF solution for 25 min at room temperature by applying a constant current density of 15 mA/cm^2 to the wafer. The porous silicon layer was then etched away in a 5 wt% NaOH solution. After the Au/Ni-Cr masking layer was removed, contacts for the piezoresistors were made by etching the nitride and oxide through contact windows. A new Au (6,000Å)/Ni-Cr (1,000Å) layer was deposited and patterned to form both the resistor pads and the mass paddle. The wafers were then annealed at 330°C in nitrogen ambient for 30 min to reduce the contact resistance of the piezoresistors and to provide good adhesion to the surface of the silicon paddle (Fig. 5(e), (f)).

Finally, the solder mass was loaded on the mass paddle by dispensing a Pb/Sn/Ag (Pb:Sn:Ag=35:63:2) solder paste[14] and the die was then heated using a reflow soldering process to form a solder ball on top of the Au/Ni-Cr mass paddle (Fig. 5(g)). The completed accelerometer consisted of a loaded mass at the center of the structure, eight beams supporting the mass, eight piezoresistors located on the beams, and eight fixed resistors outside the beams. The radius of the mass paddle (the region suspended by the eight beams in full symmetry) was 500 μm. The length, width, and thickness of the beams were 350 μm, 100 μm, and 5 μm, respectively. The air gap between the microstructure and substrate was 20 μm and the overall size of the chip was 3.7 mm × 3.7 mm.

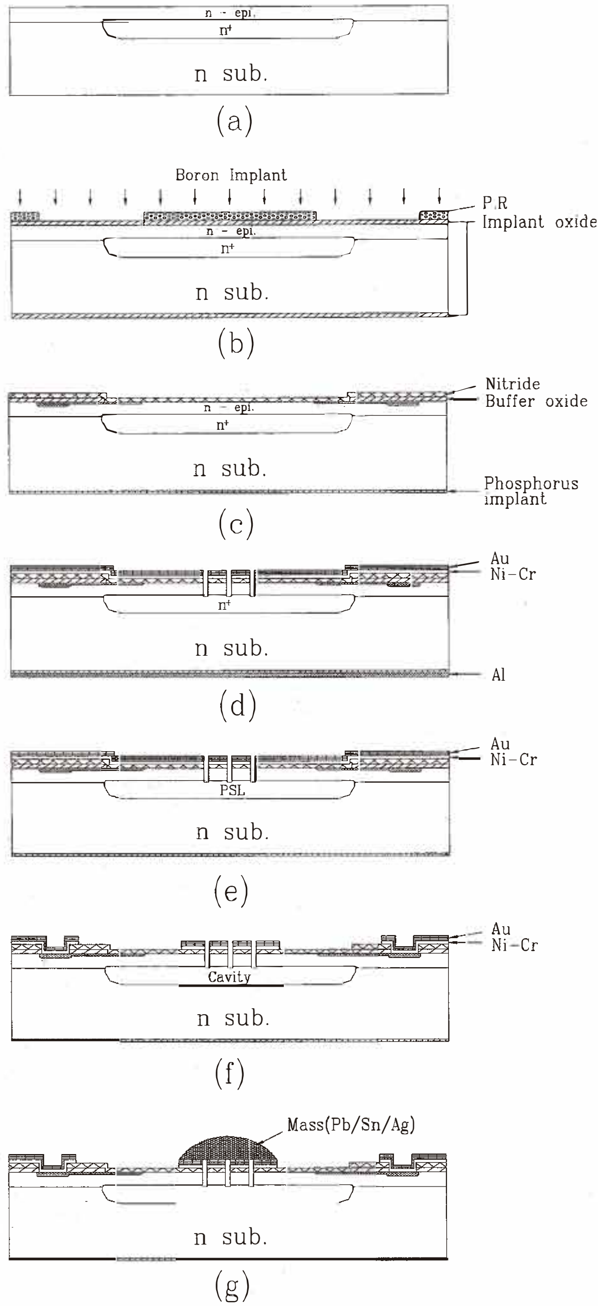

Fig. 5. Fabrication process of the silicon accelerometer.

3.2 *Results and discussion*

Surface and cross-sectional SEM views of the fabricated microstructure of the accelerometer are shown in Fig. 6. Since the anodic reaction did not proceed to the lightly doped n-type substrate, the reaction stopped automatically after the complete conversion of the n^+-region to porous silicon. The resultant microstructure shown in Fig. 6(b) was thus well defined and uniform with no cusp or any evidence of the undercutting phenomenon. This indicates that the beam thickness and the air gap height of the microstructure can be precisely adjusted by controlling the thicknesses of the n-epitaxial layer and n^+-diffused layer, respectively.

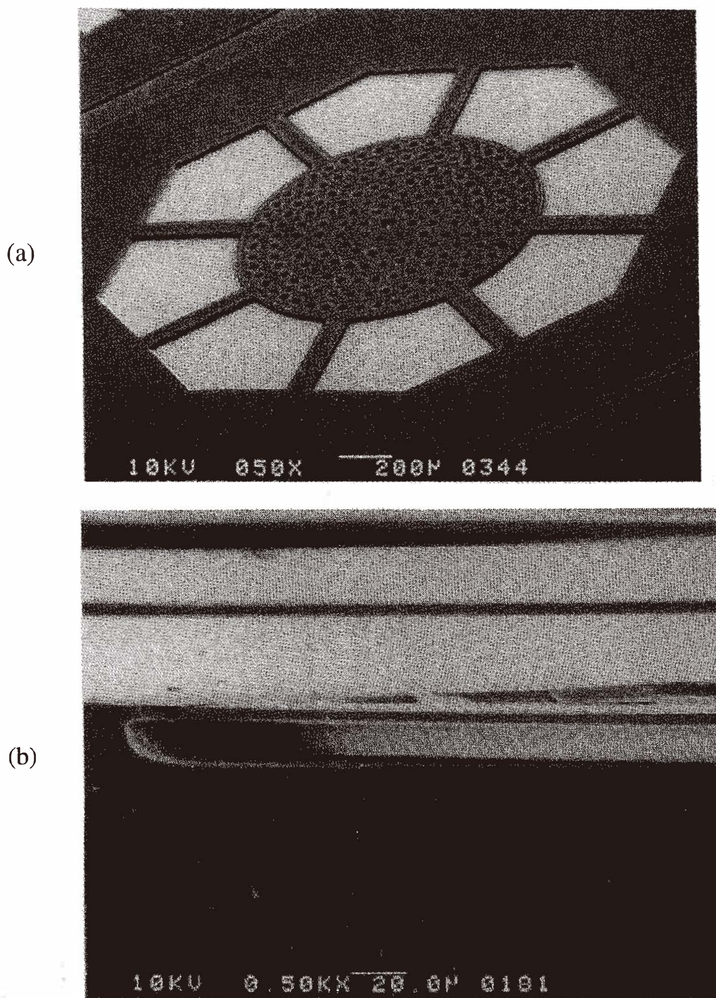

Fig. 6. Surface and cross-sectional SEM views of the 8-beam microstructure: (a) × 50 and (b) × 500.

It is known that beams are mainly formed in the <110> direction on a (100) substrate since piezoresistive coefficients are maximum in the <110> direction. Thus, in the case of a (100) plane, p-type resistors must be carefully placed along a <110> direction. On the other hand, the positioning of p-type resistors on a (111) plane is not critical because piezoresistive coefficients for longitudinal as well as for transverse stresses are the circular symmetry of all the crystal directions in this plane.[15]

Figure 7 shows a (100) and a (111) silicon wafers that have various cleavage planes cutting a crystal.[16] When we break or cleave a silicon wafer, it will cleave along the <110> direction between (111) planes, separating or breaking (110) bonds. In the case of the (100) silicon slice there are two cleavage planes 90 degrees apart, whereas in the case of the (111) slice there are three cleavage planes 120 degrees apart. Figure 8 shows the accelerometers with 4 beams on a (100) substrate and 8 beams on a (111) substrate. Usually, stress is concentrated at the edges of beams when force is applied to an accelerometer. In the case of the (100) plane, the edges of the beams are parallel to the <110> cleavage direction and thus the beams can be easily broken at the edges. However, in the case of the (111) plane, we can see that the edges of the beams are not parallel to the <110> cleavage direction since the beams can be placed in all the crystal directions; hence, the beams will not fracture easily. Consequently, microstructures formed on a (111) substrate are mechanically stronger than those fabricated on a (100) substrate because the fracture strength can be stronger according to the geometry of the beams on the wafer.

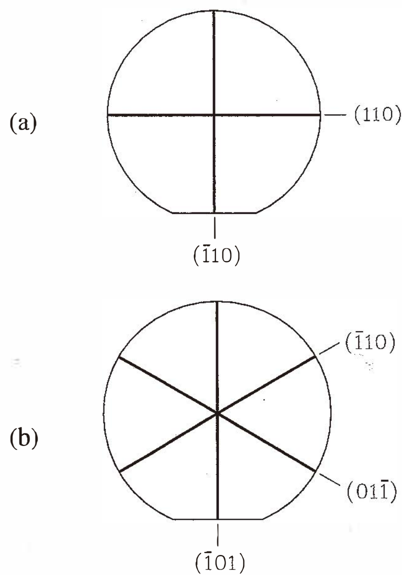

Fig. 7. The (100) and (111) silicon wafers that have various cleavage planes cutting a crystal. (a) Natural cleavage of (100) substrate and (b) natural cleavage of (111) substrate.

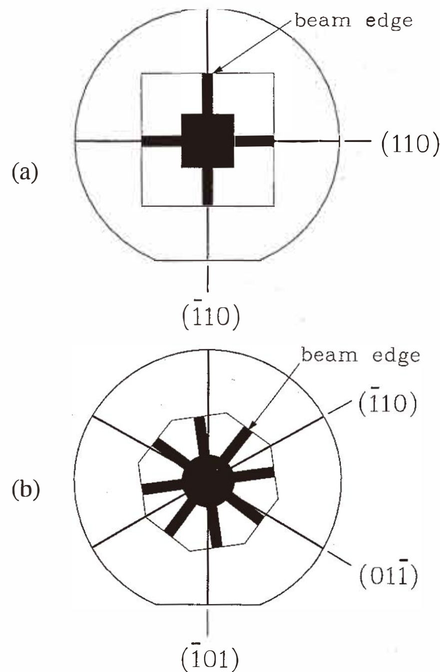

Fig. 8. The accelerometers with 4 beams on a (100) substrate and 8 beams on a (111) substrate. (a) 4-beam accelerometer on a (100) substrate and (b) 8-beam accelerometer on a (111) substrate.

Figure 9 shows a SEM image of the fabricated accelerometer. A hemispherical solder ball with a mass of about 2 mg was formed on the top of the Au/Ni-Cr mass paddle. The method of mass loading suggested in this study offers another advantage that various masses of shape or weight can be formed on the same silicon chip simply by changing the shape of the mass paddle or the dispensing rate of the solder. It is, therefore, possible to fabricate silicon accelerometers with a customized mass according to acceleration from low to high range because the mass is loaded after the other device fabrication processes are completed.

The output response of the fabricated devices has been measured by summing the four outputs of the four half-bridges, which consisted of two piezoresistors located on the beams of opposite sides and two fixed resistors outside the beams. Figure 10 shows a summing circuit for signal conditioning of the fabricated accelerometer. A constant 5 V was applied across the bridge, and the voltage differences between each bridge were amplified at the first-stage differential amplifier with a gain of 200. The outputs of the four bridges (inputs of the summing circuit) were then added at the second stage summing circuit with a unity gain.

The characteristics of the fabricated devices were evaluated with a calibration system using a high-precision reference accelerometer (B&K 4366). The fabricated accelerometer and the reference accelerometer were both placed on the same vibration exciter and the output responses of the sensors were measured using a FFT spectrum analyzer.

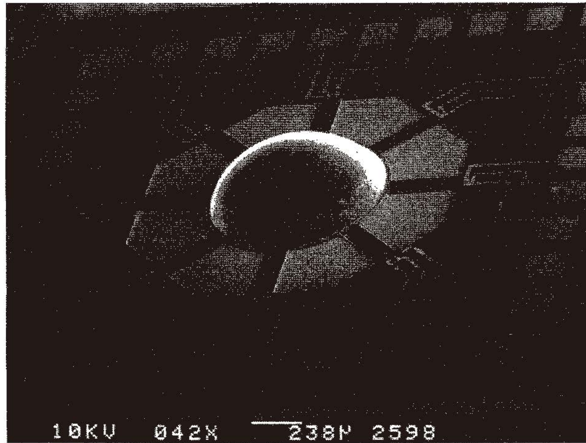

Fig. 9. SEM image of the accelerometer with the loaded seismic mass.

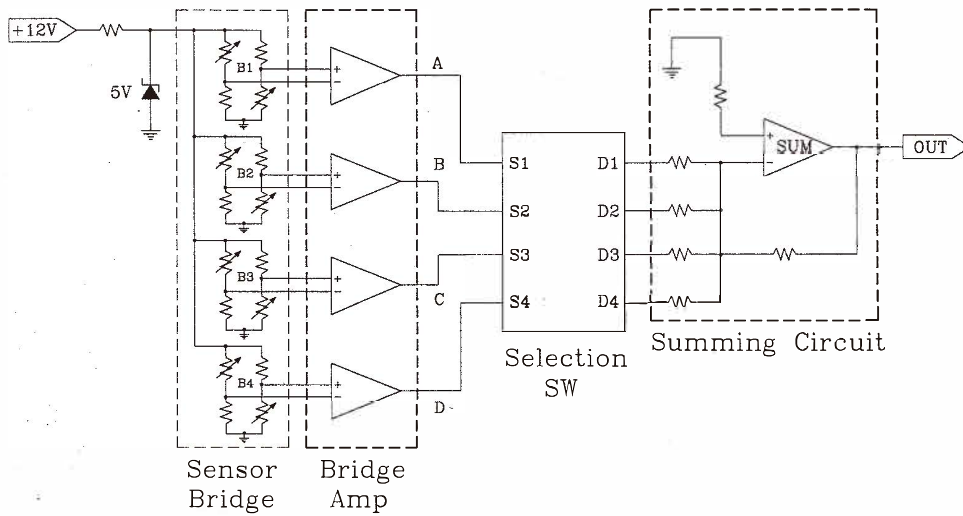

Fig. 10. Block diagram of the electronic circuitry with a summing circuit for signal conditioning of the accelerometer.

The measured result in Fig. 11 shows the output of the accelerometer sinusoidally excited with 10 G at 50 Hz. No distortion was observed in the output signal of the device, similar to the reference sensor. Figure 12 shows a linear characteristic for the device in the acceleration range from 0 to 10 G. The output deviation of each bridge was ±4%, possibly due to a misalignment between the two centers of the mass and the mass paddle, and variations in the piezoresistors. The sensitivity measured through the summing circuit was 1.21 mV/G and the nonlinearity of the sensor was less than 2% in our measurement range. When our sensor is compared with a two- or four-beam bridge-type accelerometer reported by others, the sensitivity of our device is decreased due to the additional beams. For example, the output voltage of one half-bridge of an eight-beam accelerometer is one-quarter of that of a two-beam sensor. If the four output signals of the four half-bridges are totalled through the summing circuit in Fig. 10, the total output will be equal to that of the two-beam accelerometer. Therefore, the lowering of the sensitivity due to the eight beams can be simply compensated by summing the four output signals of the four half-bridges through a summing circuit. Furthermore, the eight-beam structure provides a lower cross-axis sensitivity than two- or four-beam structures and is mechanically more stable due to a lower shear stress. In general, the sensitivity of a typical piezoresistive accelerometer for airbag applications is obtained between a few hundred μV/G and several mV/G. Therefore, we can estimate that the obtained sensitivity of this accelerometer (1.21 mV/G) is sufficient for airbag applications.

The cross-axis sensitivity measured through the summing circuit was found to be less than 3.5% in all eight beam directions on the surface. It is believed that this was caused by upward shifting of the center of mass along the z axis due to a one-side loaded mass. When the vibrating magnitude was approximately 1 G, the excitation frequency varied from 10 Hz to 3.2 kHz, as shown in Fig. 13. The measured first resonant frequency was about 2.82 kHz, a 6% lower value than the designed frequency. It was found that an error in the loaded mass is the major source of discrepancy between the estimated and the measured resonant frequency.

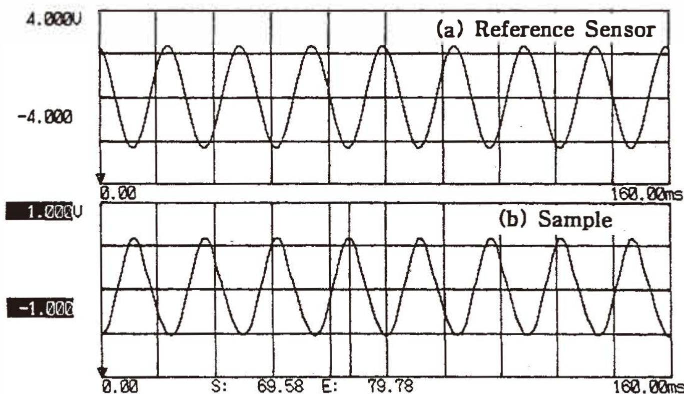

Fig. 11. Output signal to sine excitation with an amplitude of 10 G at 50 Hz.

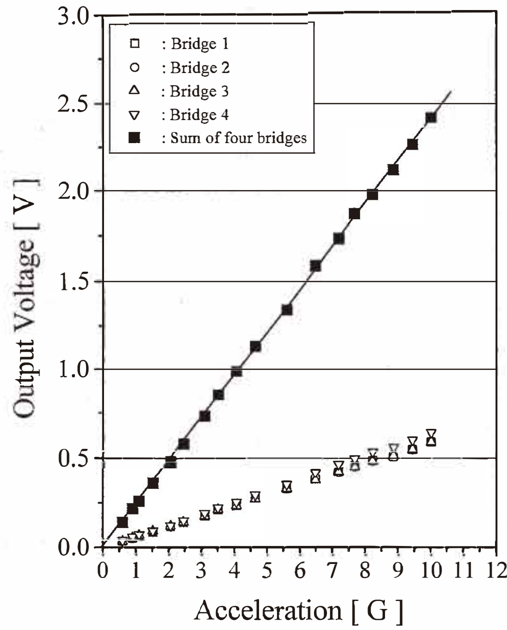

Fig. 12. Linearity of the accelerometer response for the acceleration range 0 to 10 G and a voltage amplification gain of 200.

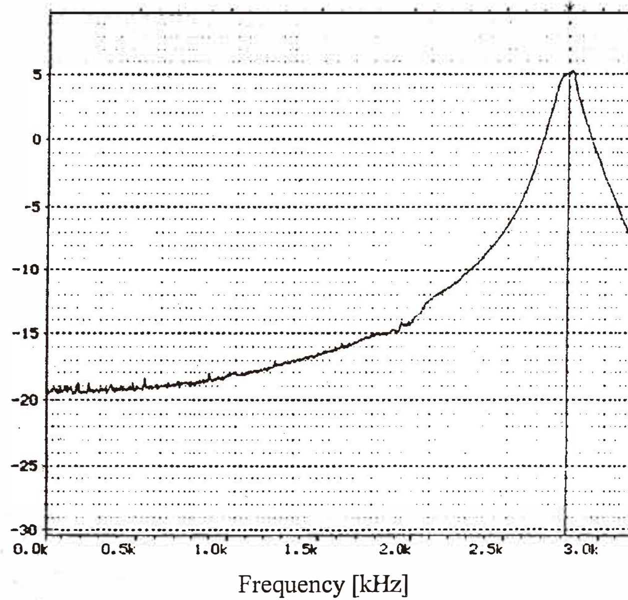

Fig. 13. Output response as a function of the excitation frequency as measured at a constant excitation of 1 G.

4. Conclusions

We have shown that the porous silicon etching method has made it possible to precisely define the dimensions of the beam and air gap in a microstructure by controlling the thickness of the n-epitaxial and n$^+$-diffusion layers on a mechanically strong (111)-oriented n/n$^+$/n structure. We are convinced that this micromachining technique provides a means of fabricating monocrystalline silicon microstructures for micromechanical applications. A bridge-type piezoresistive accelerometer with eight beams fabricated using selective porous silicon micromachining and mass loading methods has also been presented. The mechanical strength of an accelerometer can be greatly improved by adopting an eight-beam structure. The lower sensitivity of this device, compared with two- or four-beam bridge-type accelerometers, can be easily overcome by summing the four bridge output signals through a summing circuit.

Acknowledgments

The authors would like to express their thanks to Dong-Ki Kim, Dong-Kwon Kim and Jae-Seung Lee for their help in developing and characterizing the accelerometer. This work was supported by the Sensor Technology Research Center (STRC).

References

1 J. C. Greenwood: J. Phys. E; Sci. Instrum. **21** (1988) 1114.
2 J. M. Giachino: Sensors and Actuators **10** (1986) 239.
3 T. Suminto: Proc. 7th Int. Conf. Solid-State Sensors and Actuators (Transducers '91) (IEEE, San Francisco, CA, 1991) p. 104.
4 H. Seidel, H. Riedel, R. Kolbeck, G. Mück, W. Kupke and M. Königer: Sensors and Actuators A **21–23** (1990) 312.
5 W. Yun, R. T. Howe and P. R. Gray: Tech. Digest, IEEE Solid-State Sensors and Actuator Workshop, (IEEE, Hilton Head Island, SC, 1992) p. 21.
6 M. E. Motamedi: IEEE Trans. Ultrason. Ferroelec. Freq. Contr. UFFC-34 (1987) 237.
7 E. Bassous: IEEE Trans. Electron Devices ED-**25** (1978) 1178.
8 R. T. Howe: J. Vac. Sci. Technol. B **6** (1988) 1809.
9 M. J. J. Theunissen: J. Electrochem. Soc. **119** (1972) 351.
10 X. Z. Tu: J. Electrochem. Soc. **135** (1988) 2105.
11 C. J. M. Eijkel, J. Branebjerg, M. Elwenspoek and F. C. M. van de Pol: Electron Dev. Lett. **11** (1990) 588.
12 W. Lang, P. Steiner and H. Sandmaier: Sensors and Actuators A **51** (1995) 31.
13 R. P. Holmstrom and J. Y. Chi: Appl. Phys. Lett. **42** (1983) 386.
14 N. Peteron: Proc. NEPCON/West '86, (Reed Exhibition Companies, Anaheim, CA, 1986) p. 619.
15 Y. Kanda: IEEE Trans. Electron Devices ED-**29** (1982) 64.
16 G. E. McGuire: Semiconductor Materials and Process Technology Handbook (Noyes Publications, New Jersey, 1988) Chap. 4.